39th IAHR WORLD CONGRESS GRANADA, SPAIN 2022 From Snow to Sea 19-24 June 2022

Proceedings of the 39th IAHR World Congress
19–24 June 2022, Granada, Spain
doi://10.3850/IAHR-39WC2521716X2022579

Numerical Modelling of Floating Debris Impact on Structures During Extreme Hydrodynamic Events

Gioele Ruffini[(1)], Riccardo Briganti[(2)], Corrado Altomare[(3)], Paolo De Girolamo[(1)], Jacob Stolle[(4)], Bahman Ghiassi[(5)] and Myrta Castellino[(1)]

[(1)] Department of Civil, Building and Environmental Engineering DICEA, Sapienza University of Rome, Via Eudossiana 18, 00184 Rome, Italy; gioele.ruffini@uniroma1.it (G.R.); paolo.degirolamo@uniroma1.it (P.D.G.); myrta.castellino@uniroma1.it (M.C.)

[(2)] Faculty of Engineering, University of Nottingham, Nottingham NG7 2RD, UK; riccardo.briganti@nottingham.ac.uk

[(3)] Department of Civil and Environmental Engineering (DECA), Universitat Politécnica de Catalunya,Jordi Girona, 08034, Barcelona, Catalunya, Spain; corrado.altomare@upc.edu

[(4)] Institut National de la Recherche Scientifique Eau Terre Environnement, 490 Rue de la Couronne, Quebec City, QC G1K 9A9, Canada; jacob.stolle@ete.inrs.ca

[(5)] School of Engineering, University of Birmingham, Birmingham B15 2TT, UK; b.ghiassi@bham.ac.uk

Abstract

Extreme hydrodynamic events, such as tsunamis, can transport debris of a very wide range of dimensions, from cohesive sediments to debris such as trees and cars. Large sized floating debris are particularly hazardous for two main reasons: (i) they can accumulate in narrow passages, such as the case of log jams at bridges, and obstruct the flow, creating potential for further flooding; (ii) they can impact directly on structures transferring significant energy to them, due to their mass and velocity, which can lead to damage and even failure. The transport and the interactions of this type of debris is studied experimentally, often in the context of tsunamis and flash floods. However, numerical studies on large floating debris impact on structures are rare. Therefore, the present study aims to address this gap by numerically modelling of the flow-debris-structure interactions. First, the experiments of Stolle et al. (2018) are simulated numerically. These experiments involve a single positively buoyant container impact a structure as a result of being transported by a dam-break flow. The numerical simulations are carried using the open source DualSPHysics model based on the Smoothed Particle Hydrodynamics method. First, the hydrodynamics results were validated with data from Stolle et al. (2018). Subsequently, DualSPHysics was coupled with the Multiphysics engine CHRONO to simulate the container and its impact on the structure. The dam break event described in Stolle et al. (2018), was generated by modelling the movement of a swing gate using the experimental time series, with the container and the structure positioned at 3.2 m and 7.03 m, respectively, downstream of the reservoir consistently with Stolle et al. (2018). The trajectory as well as the velocity of the centroid of the container were tracked throughout the simulation. The agreement between the model and the experiment results is quantitatively assessed and it is shown that the model is accurate in reproducing the floating container trajectory, impact velocity and, in turn, force. In a second stage, numerical simulations beyond the conditions tested by Stolle et al. (2018) are used to investigate the role of the flow velocity, impact angle and location.

Keywords: Debris; DualSPHysics; Flow–debris interaction; SPH; Tsunami flooding

1. INTRODUCTION

Several major tsunamis occurred in the Pacific Ocean in recent years (Mori et al., 2011; Sassa et al. 2019), the latest of which occurred the 15th of January 2022 in Tonga, often resulted in catastrophic consequences for coastal communities and structures causing many casualties. While many studies in the literature often focused on tsunami inundation and their effect on the coastal region (e.g. Titov and Synolakis, 1997; Mori et al., 2011; Romano et al. 2020; Tonini et al. 2021), recently there has been a growing interest in investigating the effects and damage caused by waterborne debris transported by the tsunamis flows in urbanised coastal area. Many studies were conducted after the documented building damages during the 2011 Tohoku tsunami where Naito et al. (2014) developed a debris hazard classification system analysing the damages caused by different debris types. Among of the most energetic impacts are those with shipping containers, with estimated forces up to 6400 kN (Naito et al., 2014), according to FEMA P646 (2012) using the Haehnel and Daly (2004) relationship.
The American Society for Civil Engineers (ASCE, 2016) further incorporated in their design codes the effect of impact orientation of Haehnel and Daly (2004). However, not all debris materials characteristics are taken into

account in these design guidelines, which may significantly affect the impact forces as they influence the debris behaviour in the flow. For the aforementioned reason, a number of experimental studies recently focused on debris trajectories, spreading, orientation (Imamura et al. 2008; Rueben et al. 1015; Nistor et al. 2017; Stolle et al. 2018b,2020) or on analysing the forces developed during their impact with structures (Nouri et al. 2010; Riggs et al. 2014; Ikeno et al. 2016; Shaifei et al. 2016). In the two-paper series Derschum et al. (2018) and Stolle et al. (2018) modelled a 1:40 geometrically scaled 20 ft standard container, subject to a dam-break flow, and measured trajectories and impact forces on a structure, aiming at improving the reliability of design guidelines for structures and being a benchmark test for future numerical simulations.

The numerical modelling of these processes is rare in the literature (Nistor et al., 2017b). Initial studies of interaction between fluid and solids were performed by using Reynolds Averaged Navier Stokes Equations, with the Volume of Fluid tracking method, coupled with a Discrete Element Method model (DEM) (Wu et al., 2014) and validated with laboratory experiments. However, applying this class of numerical model is usually very challenging due to the use of meshes in Eulerian numerical models (Chen et al. 2020), associated with very long processing times and the difficulty of dealing with topological changes. Lagrangian particle-based methods, such as the Moving Particle Semi-implicit (MPS) method (Koshizuka and Oka, 1996) or the Smoothed Particle Hydrodynamics (SPH) method (Monaghan, 1992) gained substantial popularity in the scientific community, due to their formulation, well suited to investigate high energy phenomena such as tsunamis or violent flows (Tan et al., 2018, Pringgana et al. 2021). However, SPH requires coupling with other models to simulate interaction with solid bodies in the flow. Canelas et al. (2018) coupled DualSPHysics (Dominiguez et al., 2021) and the multiphysics solver CHRONO (Tasora et al. 2011; Anitescu et al. 2010) for this purpose. This was used to assess the feasibility of simulating floating bodies in extreme hydrodynamic events with that approach (Ruffini et al., 2021). We hereinafter present further developments of this study.
DualSPHysics (Dominiguez et al., 2021) is chosen due to the computational efficiency of the CUDA language which allows the simulation to run on GPU with major simulation speed increase with respect to CPU speed (up to 146 times, Crespo et al., 2015). CHRONO (Tasora et al. 2011; Anitescu et al. 2010) is a Differential Variational Inequality (DVI) based model that allows to solve rigid or deformable contacts and impacts between solids including a full Coulomb sliding/sticking/rolling model. In addition, it includes the possibility of integrating different types of structural constraints (Canelas et al., 2018; Tagliafierro et al. 2021). In this study, the simulations of Ruffini et al. (2021) are further expanded by including the use of the Modified Dynamic Boundary Conditions (MDBC, English et al. 2021) in their numerical setup to more accurately reproduce the fluid-floating-structure interaction. First, the modelling of the hydrodynamics of the flow is validated. Subsequently, impact forces on the structure tested in Stolle et al. (2018) are simulated. Finally, the effects of the relative positioning of the container and structure on the impact forces is discussed.

The remainder of the manuscript is organized as follows: the explanation of the methodology, illustrating the numerical setup is presented in Section 2. In Section 3 the main results of the hydrodynamics validation, debris dynamics and forces validation are presented. In Section 4, the effect of the structure initial distance from the debris is presented and analysed to understand its importance on hazard assessment plans.

2. METHODOLOGY

For the present study, DualSPHysics (Dominìguez et al., 2021) coupled with CHRONO (Tasora et al., 2011; Anitescu et al., 2010) is used to solve the hydrodynamics and the collisions and interactions between container, floor and structure, simultaneously.

2.1 DualSPHysics

DualSPHysics model is based on Weakly Compressible SPH (WCSPH) with the fluid phase governed by the Navier–Stokes equations, reduced to ordinary differential equations solved in a Lagrangian framework. The conservation of mass and momentum is expressed as (Gomez-Gesteira, 2012; Violeau and Rogers, 2016):

$$\frac{\mathrm{d}\rho}{\mathrm{d}t} = -\rho\nabla\cdot\boldsymbol{v} \quad [1]$$

$$\frac{\mathrm{d}\boldsymbol{v}}{\mathrm{d}t} = -\frac{1}{\rho}\nabla p + \boldsymbol{g} + \boldsymbol{\Gamma} \quad [2]$$

where ρ is the fluid density, t is time, p is the pressure, $\boldsymbol{v}$ is the velocity vector, $\boldsymbol{g}$ is the gravitational acceleration vector (here only $g_z = -9.81$ m/s^2 is used) and $\boldsymbol{\Gamma}$ groups all the dissipative terms that can be defined by using the artificial viscosity (Monaghan, 1992) or laminar with sub-particle scale turbulence (Gotoh et al., 2001) formulations.

SPH discretises every part of the computational domain into sets of particles carrying different properties such as density, pressure, velocity, etc. In general, two steps are defined to apply Equations [1] and [2] to the SPH method, i.e., a kernel approximation and a particle approximation Liu and Liu (2003). First, any variable f of a particle a, located at $\boldsymbol{r}_a$, is represented by an integral at location $\boldsymbol{r}$:

$$f(\boldsymbol{r}_a) = \int_\Omega f(\boldsymbol{r}) W(\boldsymbol{r}_a - \boldsymbol{r}, h_p) \mathrm{d}\boldsymbol{r} \quad [3]$$

with Ω as the computation domain, W as a weighting function called smoothing kernel, which monotonically decreases with distance, and h_p as the smoothing length which determines the radius of the kernel.
In the second step, the integral in Equation (3) is approximated by interpolating the characteristics of the surrounding particles as:

$$f(\boldsymbol{r}_a) \approx \sum_b f(\boldsymbol{r}_b) \frac{m_b}{\rho_b} W_{ab} \quad [4]$$

where the summation is extended to all the particles inside the kernel. In Equation [4], $W_{ab} = W(\boldsymbol{r}_a - \boldsymbol{r}_b, h_p)$, and m_b and ρ_b are the mass and density of a neighbour particle b (located at $\boldsymbol{r}_b$). The application to derivatives of the function f is then straightforward. Equation [1] is rewritten in the SPH framework for a particle a as

$$\frac{\mathrm{d}\rho_a}{\mathrm{d}t} = \sum_b m_b \boldsymbol{v}_{ab} \cdot \nabla_a W_{ab} + \delta_\phi h_p c_0 \sum_b \Psi_{\mathrm{ab}} \cdot \nabla_a W_{ab} \cdot \frac{m_b}{\rho_b} \quad [5]$$

with δ_ϕ a free parameter, c_0 the speed of sound of the simulation and Ψ_{ab} the density diffusion term defined, in the present study, following Fourtakas et al. (2020). A more extensive analysis of the SPH governing equations and model can be found in the reference literature (e.g. Dominìguez et al. 2021).

2.1.1 MDBC boundary condition

In DualSPHysics two different solid (i.e., non-fluid) boundary conditions formulations are implemented to treat boundary particles: the Dynamic Boundary Condition (DBC) and the MDBC. The DBC is the original formulation provided for solid boundary conditions in DualSPHysics (Crespo et al., 2007). The Modified DBC, i.e. MDBC, were introduced (English et al. 2021) to overcome some of the issues of DBC such as repulsive forces leading to a gap between fluid and solid and inaccurate fluid pressure, boundary layer, and fluid velocity. The reader is referred to English et al. (2021) for details about the methodology.
The MDBC is here applied to boundary particles that are distant less than $3h_p$ from the boundary limit, which ensures that every fluid particle close to a solid boundary only interacts with particles defined by the MDBC.

2.1.2 CHRONO

The DVI solver CHRONO (Tasora et al., 2011; Anitescu et al., 2010) implemented in DualSPHysics by (Canelas et al., 2018), which is able to consider only rigid bodies, is used herein to consider the interaction and solve the collisions between container, flume floor and structure similarly as in Ruffini et al. (2021).

CHRONO can consider multiple types of structural constraints and solving collisions between rigid bodies through two alternative formulations, (i) Non-Smooth Contacts (NSMC), which considers fully rigid impacts, and (ii) SMooth Contacts (SMC) which solves deformable contacts. For this study to approximate as closely as possible the real behaviour for all materials and elements involved the latter formulation is used. SMC considers the Young's modulus E, the Poisson's ratio ν, the restitution coefficient K and the kinetic friction coefficient f_c to define material characteristics. For an in-depth definition of the coupling algorithm with DualSPHysics the author defers to Canelas et al. (2018).

2.2 Modelled Experiment and Numerical Setup

The experimental setup shown in Figure 1 consisted of a dam-break flow impacting on a single scaled container placed initially on a dry flat concrete bottom, which in turn impacted a structure placed downflow. The experiment was conducted in a 30 m x 1.5 m flume. Part of the flume was used as a 21.55 m long reservoir filled with h_0 =0.4 m. The dam-break was generated by releasing the water via a swing gate (brown rectangle in Figure 1). The flow propagated on an 8.45 m long test area with the horizontal false floor elevated by 0.2 m from the flume bottom. The swing gate structure consisted of two 0.05 m x 0.05 m metal columns

with an additional 0.03 m ledge towards the inside of the flume covered in rubber to ensure a watertight seal. Due to the gate structure the flow was slightly obstructed by 0.08 m on each side generating three-dimensional flow features (Stolle et al. 2018). The area modelled herein is shown in Figure 1, this coincides with the experimental area. Note that x = 0 m is the initial position of the waterfront, and that the y-coordinate is rotated of 180° with respect to the one from Stolle et al. (2018b). The container x-coordinate of the geometrical centre was positioned on the false floor, respectively, at $x = 3.2$ m. Here, only the case with the container positioned with its longer axis perpendicular to the flow is simulated. The container with a mass of 0.226 kg was positioned by hand before every experimental run and centred to the flume width resulting in a mean position of the geometric centre of
$x = 3.2010$ m and $y = -0.0225$ m. The trajectories of the container were measured using a camera-based object-tracking system (Stolle et al. 2018b). The structure, positioned at x = 7.03 m was 0.2 m x 0.2 m x 0.8 m with the walls made of PVC think sheets to accommodate the load cell which measured the container and flow impact forces on the structure. Wave gauges were placed at WG1 ($x = -0.1$ m), WG2 ($x = 2.0$ m), both along the axis of the flume, and WG3 ($x = 3.2$ m) at 0.14m from the wall of the flume as shown in Figure 1.

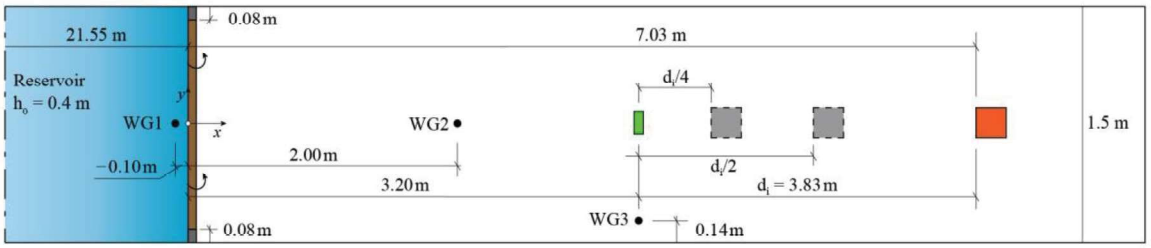

Figure 1. Experimental setup of the modelled experiments. Additional positioning of the structure investigated in the present study (not present in Stolle et al. 2018) are coloured in grey.

Note that, this is an improved version of the numerical setup of Ruffini et al. (2021). Here, contrarily to Ruffini et al. (2021) the whole experimental test area is simulated including the structure, which, in this instance, is only simulated as a rigid obstacle. The dam-break is initiated by a gate that is modelled after Stolle et al. (2018) and opened by using the mean of the experimental time series and the gate structure is approximated with two 0.05 m x 0.08 m rectangles at each side of the numerical flume. Additional runs were also carried out by changing the position of the structure as shown in Figure 1 (grey squares) at d_i /2 and d_i /4, d_i being the initial distance between container and structure in Stolle et al. (2018b).

Table 1. DualPSHysics parameters and formulations used.

Parameter	Value
dp (m)	0.01
Total number of particles	27.9 × 10^6
Smoothing kernel	Wendland (1995)
Coefh	1.2
h_p/dp	2.07
Dissipative term	Artificial viscosity (Monaghan, 1992)
α_{ff}	0.003
$visc_{bf}$	0.5
Density diffusion term	Fourtakas et al. (2020)

All boundary surfaces, including the container, are now modelled with MDBC, with the only exception being the gate, which was modelled using DBC, due stability issues of the simulation. This did not substantially impact the flow simulation due to its very fast opening. Initial inter-particle distance dp = 0.01 m was chosen following the sensitivity analysis in Ruffini et al. (2021). Additionally, note that moving to a higher resolution such as *dp*/2 was not possible without decreasing the numerical reservoir, with the current specifics of the server (Nvidia RTX A5000, 24GB RAM), due to the very large volume of the reservoir which would results in >100 million particles. Here, $h_p = \text{Coefh}\sqrt{3dp^2}$ with Coefh = 1.2, which affects the area of influence of the kernel function, was used since it is the default value for DualSPHysics. For this numerical setup the artificial viscosity formulation was used to compute the Γ term in Equation [2] (Monaghan, 1992) with the artificial viscosity parameter α_{ff} = 0.003 after initial calibration to ensure the best correspondence between simulations and experiments. This value of artificial viscosity also results in $Ma/\alpha_{ff} = 13$ where $Ma =$

$U_{ref}/c_0 = 0.04$ is the Mach number for this study considering $U_{ref} = \sqrt{g * 0.4} = 1.98$ m/s and $c_0 = 48.1$ m/s as the speed of sound of the simulation. A typical value for dam-break problems is $Ma/\alpha_{ff} \cong 10$ (Meringolo et al. 2019) which is compatible to what was used here. Additionally, in contrast to what was used in Ruffini et al. (2021) here the viscosity between fluid and boundary particles α_{bf} was kept such that $\alpha_{bf} = 0.5\alpha_{ff}$. The laminar+SPS dissipation model was also evaluated for this study but, although similar water depth results were achieved, the velocity field showed more numerical noise. All the numerical parameters and formulations used are summarised in Table 1.

All the physical characteristics of the container are calculated following Ruffini et al. (2021) including the inertia matrix. All the materials characteristics used for the container, flume floor and structure are summarised in Table 2 and assumed to be standard values for the different materials (Harper, 2000; Micheal 1991). The interaction distance between solids is defined as 1% of the particle resolution to have more accuracy during the impact of the container on the structure.

Table 2. Material properties values used with CHRONO with SMooth Contacts.

Property	Container (HMWPE)	Flume Floor (Concrete + Sand Paint)	Structure (PVC)
E (Gpa)	0.8	30	3
ν (-)	0.4	0.2	0.3
K (-)	0.7	0.7	0.7
f_c (-)	0.15	0.3	0.15

2.3 Quantification of Model Performance

The accuracy of the numerical simulations results of the flow depth (h) of the x and y trajectories of the container was assessed by using the root mean square error normalised with h_0 ($\mathrm{nRMSE_l}$) as

$$\mathrm{nRMSE_l} = \frac{\sqrt{\frac{1}{N}\sum_i^N \left(\xi_{n,i} - \xi_{e,i}\right)^2}}{h_0}, \quad [6]$$

where $\xi_{n,i}$ and $\xi_{e,i}$ represent any i-th sample of one of the numerically modelled and experimental variables, respectively, and N is the number of samples. Furthermore, the accuracy of the simulated x and y velocity components of the container (v_x and v_y, respectively) was assessed with a root mean square error normalised with the shallow water velocity ($\mathrm{nRMSE_v}$) as

$$\mathrm{nRMSE_v} = \frac{\sqrt{\frac{1}{N}\sum_i^N \left(v_{n,i} - v_{e,i}\right)^2}}{\sqrt{gh_0}}, \quad [7]$$

where $v_{n,i}$ and $v_{e,i}$ represent the numerical and experimental velocity components, respectively, in either x- or y-directions. Due to the stochastic nature of the phenomenon the impact forces of the container on the structure are also investigated and the performance of the model on reproducing their mean value is measured with a root mean square error normalised with the range of the measure experimental forces ($\mathrm{nRMSE_f}$) as

$$\mathrm{nRMSE_f} = \frac{\sqrt{\frac{1}{N}\sum_i^N \left(F_{n,i} - F_{mean-e,i}\right)^2}}{\left|F_{e,max} - F_{e,min}\right|}, \quad [8]$$

where $F_{n,i}$ represent the numerical and $F_{mean-e,i}$ represent the experimental mean force, with $F_{e,max} - F_{e,min}$ representing the experimental range of measured forces.

3. RESULTS

In this section all the results of the validation of the hydrodynamics, together with container dynamics and impact forces compared against the experiments of Stolle et la. (2018) are presented.

3.1 Hydrodynamics

The flow depth normalised with the initial water depth of the dam break flow h/h_0 is shown in Figure 2 for all three wave gauges WG1, WG2 and WG3 where in grey are represented all experimental runs, black their mean values and in red the numerical results. In all three positions the numerical model is able to reproduce h with low values of $nRMSE_I$ as summarised in Table 3.

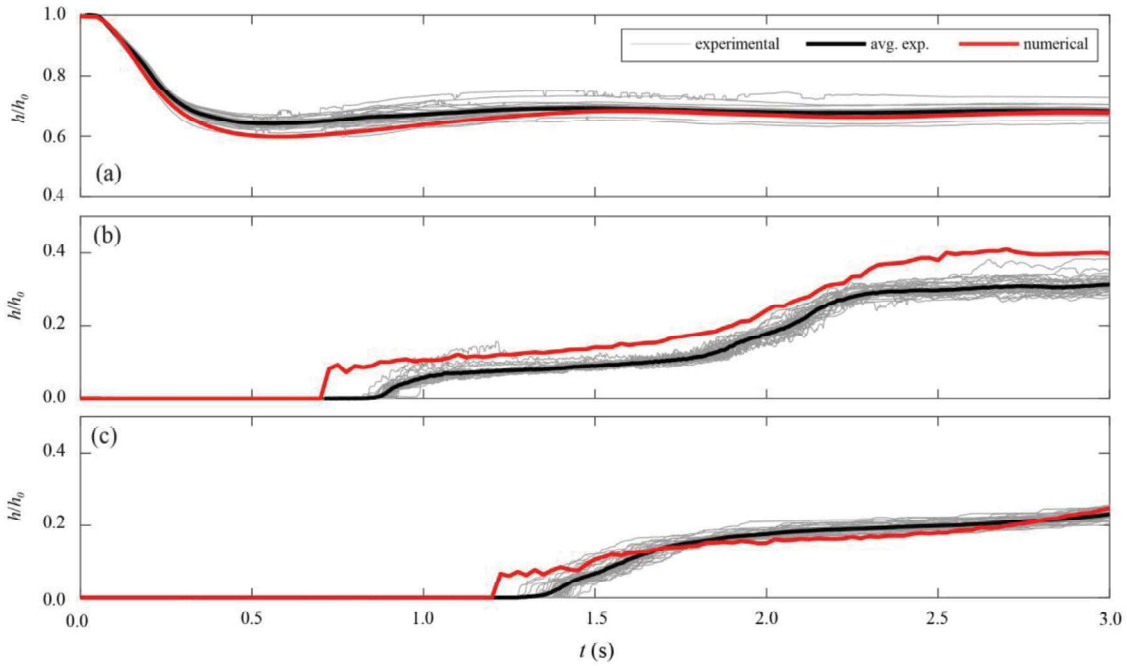

Figure 2. Comparison of h/h_0 between numerical and experimental results at: (a) WG1, (b) WG2 and (c) WG3.

The arrival time of the flow at WG3, which is at the same initial x position of the container, is right at the edge of the experimental values with a difference of t≈-0.09 s from the experimental mean. The water depth at WG2 is almost always overestimated by the numerical results. Note that WG2 and WG3 are positioned at different y positions, and the difference in agreement is mostly due to the 3D features of the flows in the experiments (Stolle et al., 2019). These features are generated by the gate structure, which here is only approximated using two rectangular shaped columns due to resolution constraints of the model. However, it must be noted that by adding MDBC and implementing a more faithful representation of the water release mechanism the overall shape of the time series is much closer to the experiments than in Ruffini et al. (2021).

Table 3. $nRMSE_I$ values for hydrodynamic characteristics of the flow at the different WGs.

	WG1	WG2	WG3
$nRMSE_I$	0.018	0.064	0.022

3.2 Container Dynamics and Trajectories

In Figure 3 the trajectories and velocities of the container in x and y directions are shown. It can be seen how the container movement (a,b) and velocities in x (c) and y (d) directions they do not perfectly match the mean experimental values but they capture the main characteristics of the container dynamics of all the experiments. The numerical container trajectory appears to be less meandering than the individual trajectories and less shifted towards positive values of y than most of the individual and mean trajectories. The $nRSME_I$ and $nRMSE_v$ value for both trajectories and velocities of the container in x- and y-direction are summarised in Table 4.

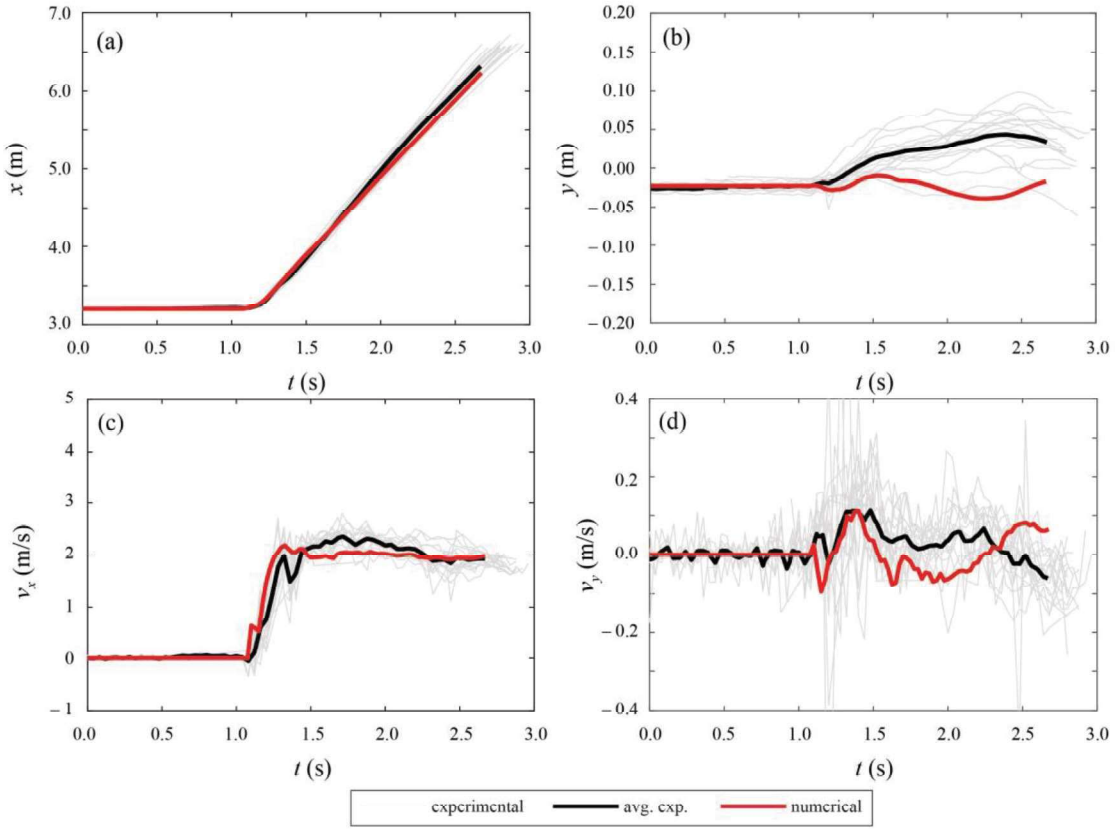

Figure 3. Comparison of the container (a,b) trajectories and (c,d) velocities time series between numerical and experimental results.

Table 4. $nRMSE_l$ and $nRMSE_v$ values for container trajectories and dynamics.

	x	y
$nRMSE_l$	0.14	0.10
	v_x	v_y
$nRMSE_v$	0.10	0.03

3.3 Impact Forces

A comparison of the impact force on the structure between simulations and experiments is presented in Figure 4. Note that the simulated impact force computed by CHRONO are extracted only in the main direction of the flow (x-direction) as $F_x = ma_x$ where m is the mass of the container and a_x is the maximum acceleration in x-direction of the container at the impact. Note that in some of the experiments in Derschum et al. (2018) the container remained trapped in the area in front of the structure for a certain amount of time causing the container hitting the structure multiple times. Something similar happens in the numerical simulation, the container impacts the structure additional times before being transported away by the dam-break flow. In Figure 4 the experimental impact forces (grey circles) are shown with their mean (horizontal black line) and compared to the simulation (horizontal red line). The experimental mean for F_x is 153.79 N, which compared to the one calculated in the simulation of 111.7 N results in a $nRMSE_f$ = 0.24. Moving by few millimetres the initial position of the container can cause the impact force to change noticeably similarly to what happens in the experiments.

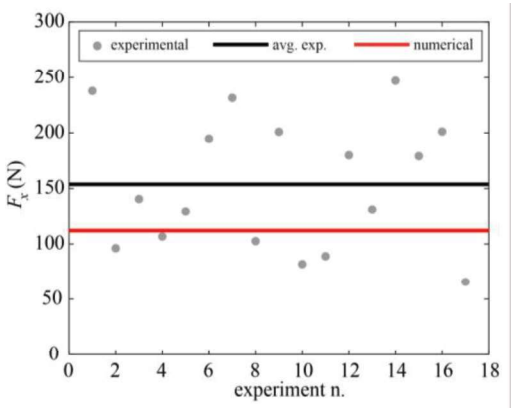

Figure 4. Comparison of the impact forces in x-direction F_x between numerical results and experimental measurements from the load cell, together with their mean value.

4. THE EFFECT OF THE CONTAINER-STRUCTURE DISTANCE ON IMPACT FORCES

Hereinafter, the effect of the position of the structure along the flume on the impact force is analysed. Figure 5 shows in the top panel how the container trajectory remains the same until the structure is impacted, after which the container is diverted on one side and surpasses the obstacle. Impact forces are then measured and reported together with the impact orientation of the container in the bottom part of Figure 5 with each letter representing a structure position. The velocity of the container in x-direction is quasi-steady at the stage of the flow in which each impact occurs (the first impact occurs at t ≈ 1.6 s) as can also be seen in Figure 3c. Due to this, the difference in impact forces can be mainly associated with the impact orientation. This explains why the impact forces for (a) and (c) positions, where the impact occurs first on a corner of the container, are smaller than (b) where the impact occurs with the entire edge. Note that this behaviour is consistent with experimental results of Stolle et al. (2018) and Derschum et al. (2018).

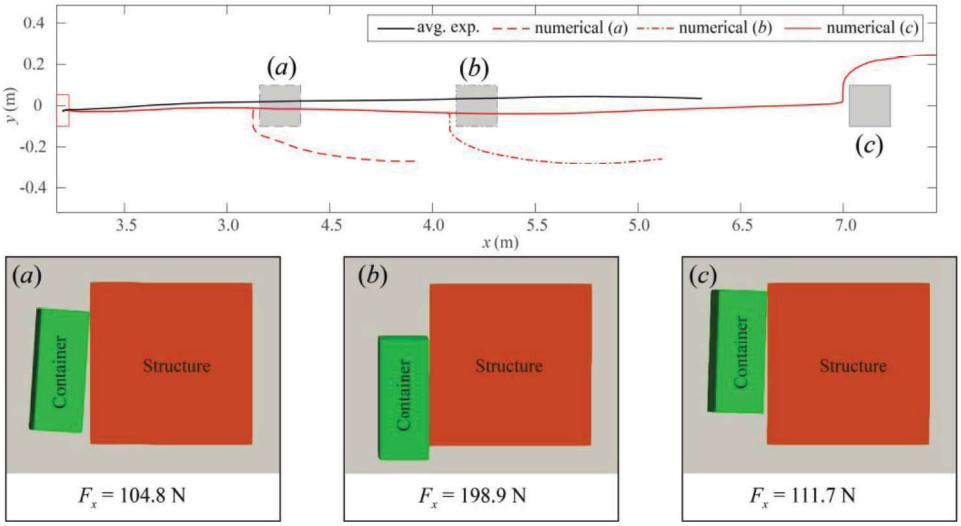

Figure 5. Comparison of container trajectories and impact forces for the three different positions of the structure (a) $d_i/4$, (b) $d_i/2$ and (c) d_i.

5. CONCLUSIONS

This study presents the validation of the simulation of the transport of a single container by a dam-break flow, together with the computation of its impact force on a structure. The addition of the opening gate, MDBC, and the coupling with CHRONO has helped to improve the results already validated in Ruffini et al. (2021). The use of the MDBC formulation helped to obtain a smoother pressure field and to eliminate the gap between solids and fluid occurring when the standard DBC are used. This also contributed to attaining a more accurate representation of the container impact on the structure. The impact force computed using the present approach is smaller than the mean force measured in Stolle et al. (2018) experiments. Consistently with experimental evidence and, as also recognised in design guidelines (FEMA, 2012), the computed impact

forces significantly vary with impact orientation in a stage of the flow in which the velocity is quasi-steady. Therefore, it is possible that small differences in the simulation of the flow lead to large differences in the angle of impact with respect to the experiments, thus explaining the underestimation. Finally, it must be noted that the structure is considered completely rigid in the present simulations, while in the experiments the PVC structure was connected to the foundation via a load cell that allowed movement. Overall, the numerical model is able to reproduce trajectories and impact forces on a rigid structure accurately, considering the approximations on the structure and the non-inclusion of air in the model. The study of the impact forces over the different structure positions has highlighted that, once the container velocity stabilises under the flow conditions, the impact orientation plays a very important role in determining the force transmitted to the structure by the floating bodies with more direct impacts resulting, as expected, in higher forces.

This study has also highlighted the role of the resolution in obtaining realistic impacts. In fact, the use of MDBC requires that debris are described by a minimum number of particles to provide realistic interactions between solids. Furthermore, dam break flows stretch on flat areas in way that the flow depth is comparable with the dimensions of the debris, so that both flow and debris need to be resolved by an adequate number of particles. These considerations prompt the development of efficient techniques of refining resolution where needed.

6. REFERENCES

American Society for Civil Engineers (ASCE). (2016). *Minimum Design Loads and Associated Criteria for Buildings and Other Structures*, ASCE/SEI 7-16.

Anitescu, M., & Tasora, A. (2010). An iterative approach for cone complementarity problems for nonsmooth dynamics. *Computational Optimization and Applications*, 47(2), 207-235.

Canelas, R. B., Brito, M., Feal, O. G., Domínguez, J. M., & Crespo, A. J. C. (2018). Extending DualSPHysics with a Differential Variational Inequality: modeling fluid-mechanism interaction. *Applied Ocean Research*, *76*, 88-97.

Chen, F., Heller, V., Briganti, R. (2020). Numerical modelling of tsunamis generated by iceberg calving validated with large-scale laboratory experiments. *Advances in Water Resources* 142:103647

Crespo, A.J.C.; Domínguez, J.M.; Rogers, B.D.; Gómez-Gesteira, M.; Longshaw, S.; Canelas, R.; Vacondio, R.; Barreiro, A.; García-Feal, O. (2015). DualSPHysics: Open-source parallel CFD solver based on Smoothed Particle Hydrodynamics (SPH). *Computer Physics Communication*, 187, 204–216.

Crespo, A.J.C.; Gómez-Gesteira, M.; Dalryple, R.A. (2007). Boundary conditions generated by dynamic particles in SPH methods. *CMC–Computers Materials and Continua*, 5, 173–184.

Derschum, C., Nistor, I., Stolle, J., & Goseberg, N. (2018). Debris impact under extreme hydrodynamic conditions part 1: Hydrodynamics and impact geometry. *Coastal Engineering*, 141, 24-35.

Domínguez, J.M, Fourtakas, G., Altomare, C., Canelas, R. B., Tafuni, A., García-Feal, O., Martínez-Estévez, I., Mokos, A., Vacondio, R., Crespo, A. J. C., Rogers, B. D., Stansby, P. K., Gómez-Gesteira, M. (2021). DualSPHysics: from fluid dynamics to Multiphysics problems. *Computation Particle Mechanics*, 1-29.

English, A., J. M. Domínguez, R. Vacondio, A. J. C. Crespo, P. K. Stansby, S. J. Lind, L. Chiapponi; M. Gómez-Gesteira (2021) Modified dynamic boundary conditions (mDBC) for general-purpose smoothed particle hydrodynamics (SPH): application to tank sloshing, dam break and fish pass problems. *Computational Particle Mechanics.*

FEMA. (2012). *Guidelines for Design of Structures for Vertical Evacuation from Tsunamis, 2nd edition*. FEMA, Washington, DC, USA, FEMA P646.

Fourtakas, G., Vacondio, R., Domínguez, J. M., & Rogers, B. D. (2020). Improved density diffusion term for long duration wave propagation. In Proceedings of the International SPHERIC Workshop, Harbin, China.

Gomez-Gesteira, M., Rogers, B. D., Crespo, A. J., Dalrymple, R. A., Narayanaswamy, M., & Dominguez, J. M. (2012). SPHysics–development of a free-surface fluid solver–Part 1: Theory and formulations. *Computers & Geosciences*, 48, 289-299.

Gotoh H, Shao S, Memita T. (2001). SPH-LES model for numerical investigation of wave interaction with partially immersed breakwater. *Coastal Engineering Journal*, 46(1), 39–63.

Haehnel, R.B., and Daly, S.F. (2004). Maximum impact force of woody debris on flood plain structures. *Journal of Hydraulic Engineering*. 130, 112–120.

Harper, Charles A. (2000). *Modern plastics handbook*. McGraw Hill Professional, 2000

Imamura, F., Goto, K., & Ohkubo, S. (2008). A numerical model for the transport of a boulder by tsunami. *Journal of Geophysical Research: Oceans*, 113(C1).

Ikeno, M., Takabatake, D., Kihara, N., Kaida, H., Miyagawa, Y., & Shibayama, A. (2016). Improvement of collision force formula for woody debris by airborne and hydraulic experiments. *Coastal Engineering Journal*, 58(04), 1640022.

Koshizuka, S., & Oka, Y. (1996). Moving-particle semi-implicit method for fragmentation of incompressible fluid. *Nuclear science and engineering*, 123(3), 421-434.

Liu, G.R.; Liu, M.B. (2003). *Smoothed Particle Hydrodynamics: A meshfree particle method*, Edition Number; World Scientific: Singapore.
Michael L. Berins (1991). *SPI Plastics Engineering Handbook of the Society of the Plastics Industry*, Inc., Springer
Monaghan, J. J. (1992). Smoothed particle hydrodynamics. *Annual review of astronomy and astrophysics*, 30(1), 543-574.
Mori, N., Takahashi, T., Yasuda, T., & Yanagisawa, H. (2011). Survey of 2011 Tohoku earthquake tsunami inundation and run-up. Geophysical research letters, 38(7).
Naito, C., Cercone, C., Riggs, H. R., & Cox, D. (2014). Procedure for site assessment of the potential for tsunami debris impact. *Journal of Waterway, Port, Coastal, and Ocean Engineering*, 140(2), 223-232.
Nistor, I., Goseberg, N., Stolle, J., Mikami, T., Shibayama, T., Nakamura, R., & Matsuba, S. (2017). Experimental investigations of debris dynamics over a horizontal plane. *Journal of Waterway, Port, Coastal, and Ocean Engineering*, 143(3), 04016022.
Nistor, I., Goseberg, N., & Stolle, J. (2017b). Tsunami-driven debris motion and loads: A critical review. *Frontiers in Built Environment*, 3, 2.
Nouri, Y., Nistor, I., Palermo, D., & Cornett, A. (2010). Experimental investigation of tsunami impact on free standing structures. *Coastal Engineering Journal*, 52(01), 43-70.
Pringgana, G., Cunningham, L. S., & Rogers, B. D. (2021). Influence of orientation and arrangement of structures on Tsunami impact forces: numerical investigation with smoothed particle hydrodynamics. *Journal of Waterway, Port, Coastal, and Ocean Engineering*, *147*(3), 04021006.
Riggs, H. R., Cox, D. T., Naito, C. J., Kobayashi, M. H., Piran Aghl, P., Ko, H. S., & Khowitar, E. (2014). Experimental and analytical study of water-driven debris impact forces on structures. *Journal of Offshore Mechanics and Arctic Engineering*, 136(4).
Romano, A., Lara, J.L., Barajas, G., Di Paolo, B., Bellotti, G., Di Risio, M., Losada, I.J. and De Girolamo, P., 2020. Tsunamis Generated by Submerged Landslides: Numerical Analysis of the Near-Field Wave Characteristics. *Journal of Geophysical Research: Oceans*, 125(7).
Rueben, M., Cox, D., Holman, R., Shin, S., & Stanley, J. (2015). Optical measurements of tsunami inundation and debris movement in a large-scale wave basin. *Journal of Waterway, Port, Coastal, and Ocean Engineering*, 141(1), 04014029.
Ruffini G, Heller V, Briganti R.; (2021). Numerical characterisation and efficient prediction of landslide-tsunami propagation over a wide range of idealised bathymetries. *Coastal Engineering*, 103854.
Sassa, S., & Takagawa, T. (2019). Liquefied gravity flow-induced tsunami: first evidence and comparison from the 2018 Indonesia Sulawesi earthquake and tsunami disasters. *Landslides*, 16(1), 195-200.
Stolle, J., Derschum, C., Goseberg, N., Nistor, I., & Petriu, E. (2018). Debris impact under extreme hydrodynamic conditions part 2: Impact force responses for non-rigid debris collisions. *Coastal Engineering*, 141, 107-118.
Stolle, J., Goseberg, N., Nistor, I., & Petriu, E. (2018b). Probabilistic investigation and risk assessment of debris transport in extreme hydrodynamic conditions. *Journal of Waterway, Port, Coastal, and Ocean Engineering*, 144(1), 04017039.
Stolle, J., Ghodoosipour, B., Derschum, C., Nistor, I., Petriu, E., & Goseberg, N. (2019). Swing gate generated dam-break waves. *Journal of Hydraulic Research*, 57(5), 675-687.
Stolle, J., Nistor, I., Goseberg, N., & Petriu, E. (2020). Multiple Debris Impact Loads in Extreme Hydrodynamic Conditions. *Journal of Waterway, Port, Coastal, and Ocean Engineering*, 146(2), 04019038.
Tagliafierro B., Mancini S., Ropero-Giralda P., Domínguez J.M., Crespo A.J.C., Viccione G. (2021) Performance Assessment of a Planing Hull Using the Smoothed Particle Hydrodynamics Method. *Journal of Marine Science and Engineering*; 9(3):244.
Tan, H., Ruffini, G., Heller, V., & Chen, S. (2018). A numerical landslide-tsunami hazard assessment technique applied on hypothetical scenarios at Es Vedrà, offshore Ibiza. *Journal of Marine Science and Engineering*, 6(4), 111.
Tasora, A., & Anitescu, M. (2011). A matrix-free cone complementarity approach for solving large-scale, nonsmooth, rigid body dynamics. *Computer Methods in Applied Mechanics and Engineering*, 200(5-8), 439-453.
Titov, V. V., & Synolakis, C. E. (1997). Extreme inundation flows during the Hokkaido-Nansei-Oki tsunami. *Geophysical Research Letters*, *24*(11), 1315-1318.
Tonini R, Di Manna P, Lorito S, Selva J, Volpe M, Romano F, Basili R, Brizuela B, Castro MJ, de la Asunción M, Di Bucci D, Dolce M, Garcia A, Gibbons SJ, Glimsdal S, González-Vida JM, Løvholt F, Macías J, Piatanesi A, Pizzimenti L, Sánchez-Linares C and Vittori E (2021) Testing Tsunami Inundation Maps for Evacuation Planning in Italy. *Front. Earth Sci.* 9:628061.
Violeau, D.; Rogers, B.D. (2016). Smoothed Particle Hydrodynamics (SPH) for free-surface flows: Past, present and future. *Journal of Hydraulic Research*, 54, 1–26.
Wendland, H. (1995). Piecewise polynomial, positive definite and compactly supported radial functions of minimal degree. *Advances in computational Mathematics*, 4(1), 389-396.
Wu, T. R., Chu, C. R., Huang, C. J., Wang, C. Y., Chien, S. Y., & Chen, M. Z. (2014). A two-way coupled simulation of moving solids in free-surface flows. *Computers & Fluids*, 100, 347-355.

